Complex thermoelectric materials

Thermoelectric materials, which can generate electricity from waste heat or be used as solid-state Peltier coolers, could play an important role in a global sustainable energy solution. Such a development is contingent on identifying materials with higher thermoelectric efficiency than available at present, which is a challenge owing to the conflicting combination of material traits that are required. Nevertheless, because of modern synthesis and characterization techniques, particularly for nanoscale materials, a new era of complex thermoelectric materials is approaching. We review recent advances in the field, highlighting the strategies used to improve the thermopower and reduce the thermal conductivity.

G. JEFFREY SNYDER* AND ERIC S. TOBERER

Materials Science, California Institute of Technology, 1200 East California Boulevard, Pasadena, California 91125, USA

***e-mail: jsnyder@caltech.edu**

The world's demand for energy is causing a dramatic escalation of social and political unrest. Likewise, the environmental impact of global climate change due to the combustion of fossil fuels is becoming increasingly alarming. One way to improve the sustainability of our electricity base is through the scavenging of waste heat with thermoelectric generators (Box 1). Home heating, automotive exhaust, and industrial processes all generate an enormous amount of unused waste heat that could be converted to electricity by using thermoelectrics. As thermoelectric generators are solid-state devices with no moving parts, they are silent, reliable and scalable, making them ideal for small, distributed power generation[1]. Efforts are already underway to replace the alternator in cars with a thermoelectric generator mounted on the exhaust stream, thereby improving fuel efficiency[2]. Advances in thermoelectrics could similarly enable the replacement of compression-based refrigeration with solid-state Peltier coolers[3].

Thermoelectrics have long been too inefficient to be cost-effective in most applications[4]. However, a resurgence of interest in thermoelectrics began in the mid 1990s when theoretical predictions suggested that thermoelectric efficiency could be greatly enhanced through nanostructural engineering, which led to experimental efforts to demonstrate the proof-of-principle and high-efficiency materials[5,6]. At the same time, complex bulk materials (such as skutterudites[7], clathrates[8] and Zintl phases[9]) have been explored and found that high efficiencies could indeed be obtained. Here, we review these recent advances, looking at how disorder and complexity within the unit cell as well as nanostructured materials can lead to enhanced efficiency. This survey allows us to find common traits in these materials, and distill rational design strategies for the discovery of materials with high thermoelectric efficiency. More comprehensive reviews on thermoelectric materials are well covered in several books[1,10–12] and articles[3,5,6,8,13–18].

CONFLICTING THERMOELECTRIC MATERIAL PROPERTIES

Fundamental to the field of thermoelectric materials is the need to optimize a variety of conflicting properties. To maximize the thermoelectric figure of merit (zT) of a material, a large thermopower (absolute value of the Seebeck coefficient), high electrical conductivity, and low thermal conductivity are required. As these transport characteristics depend on interrelated material properties, a number of parameters need to be optimized to maximize zT.

CARRIER CONCENTRATION

To ensure that the Seebeck coefficient is large, there should only be a single type of carrier. Mixed n-type and p-type conduction will lead to both charge carriers moving to the cold end, cancelling out the induced Seebeck voltages. Low carrier concentration insulators and even semiconductors have large Seebeck coefficients; see equation (1). However, low carrier concentration also results in low electrical conductivity; see equation (2). The interrelationship between carrier concentration and Seebeck coefficient can be seen from relatively simple models of electron transport. For metals or degenerate semiconductors (parabolic band, energy-independent scattering approximation[19]) the Seebeck coefficient is given by:

$$\alpha = \frac{8\pi^2 k_B^2}{3eh^2} m^* T \left(\frac{\pi}{3n}\right)^{2/3} , \qquad (1)$$

where n is the carrier concentration and m^* is the effective mass of the carrier.

The electrical conductivity (σ) and electrical resistivity (ρ) are related to n through the carrier mobility μ:

$$1/\rho = \sigma = ne\mu . \qquad (2)$$

Figure 1a shows the compromise between large thermopower and high electrical conductivity in thermoelectric materials that must be struck to maximize the figure of merit zT ($\alpha^2\sigma T/\kappa$), where κ is the thermal conductivity. This peak typically occurs at carrier concentrations between 10^{19} and 10^{21} carriers per cm^3 (depending on the material system), which falls in between common metals and semiconductors — that is, concentrations found in heavily doped semiconductors.

EFFECTIVE MASS

The effective mass of the charge carrier provides another conflict as large effective masses produce high thermopower but low electrical conductivity. The m^* in equation (1) refers to the density-of-states

effective mass, which increases with flat, narrow bands with high density of states at the Fermi surface. However, as the inertial effective mass is also related to m^*, heavy carriers will move with slower velocities, and therefore small mobilities, which in turn leads to low electrical conductivity (equation (2)). The exact relationship between effective mass and mobility is complex, and depends on electronic structure, scattering mechanisms and anisotropy. In principle, these effective mass terms can be decoupled in anisotropic crystal structures[20].

A balance must be found for the effective mass (or bandwidth) for the dominant charge carrier, forming a compromise between high effective mass and high mobility. High mobility and low effective mass is typically found in materials made from elements with small electronegativity differences, whereas high effective masses and low mobilities are found in materials with narrow bands such as ionic compounds. It is not obvious which effective mass is optimum; good thermoelectric materials can be found within a wide range of effective masses and mobilities: from low-mobility, high-effective-mass polaron conductors (oxides[14], chalcogenides[21]) to high-mobility, low-effective-mass semiconductors (SiGe, GaAs).

ELECTRONIC THERMAL CONDUCTIVITY

Additional materials design conflicts stem from the necessity for low thermal conductivity. Thermal conductivity in thermoelectrics comes from two sources: (1) electrons and holes transporting heat (κ_e) and (2) phonons travelling through the lattice (κ_l). Most of the electronic term (κ_e) is directly related to the electrical conductivity through the Wiedemann–Franz law:

$$\kappa = \kappa_e + \kappa_l \tag{3a}$$

and

$$\kappa_e = L\sigma T = ne\mu LT\,, \tag{3b}$$

where L is the Lorenz factor, 2.4×10^{-8} J^2 K^{-2} C^{-2} for free electrons.

Box 1 Thermoelectric devices

The thermoelectric effects arise because charge carriers in metals and semiconductors are free to move much like gas molecules, while carrying charge as well as heat. When a temperature gradient is applied to a material, the mobile charge carriers at the hot end tend to diffuse to the cold end. The build-up of charge carriers results in a net charge (negative for electrons, e^-, positive for holes, h^+) at the cold end, producing an electrostatic potential (voltage). An equilibrium is thus reached between the chemical potential for diffusion and the electrostatic repulsion due to the build-up of charge. This property, known as the Seebeck effect, is the basis of thermoelectric power generation.

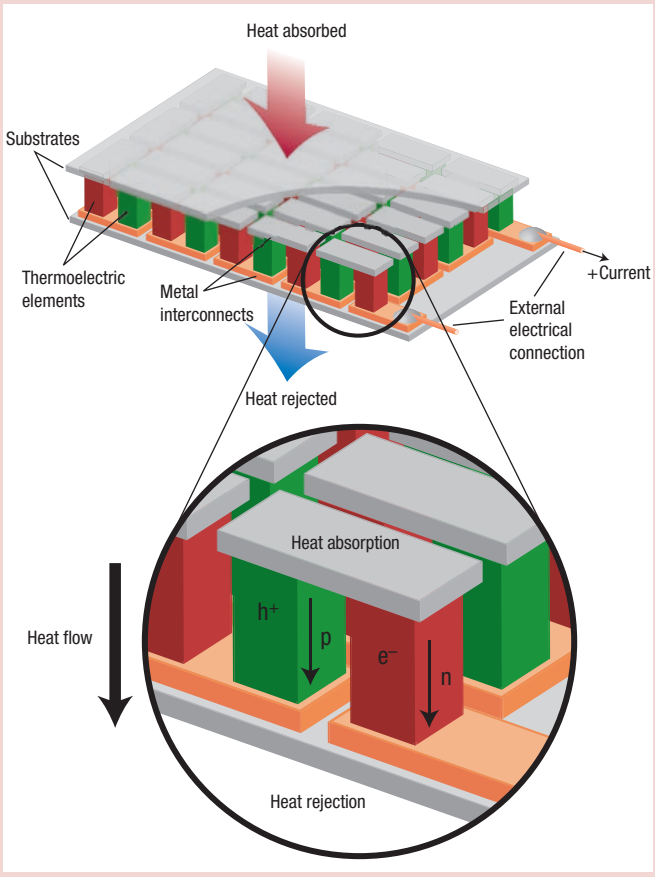

Figure B1 Thermoelectric module showing the direction of charge flow on both cooling and power generation.

Thermoelectric devices contain many thermoelectric couples (Fig. B1, bottom) consisting of n-type (containing free electrons) and p-type (containing free holes) thermoelectric elements wired electrically in series and thermally in parallel (Fig. B1, top). A thermoelectric generator uses heat flow across a temperature gradient to power an electric load through the external circuit. The temperature difference provides the voltage ($V = \alpha\Delta T$) from the Seebeck effect (Seebeck coefficient α) while the heat flow drives the electrical current, which therefore determines the power output. In a Peltier cooler the external circuit is a d.c. power supply, which drives the electric current (I) and heat flow (Q), thereby cooling the top surface due to the Peltier effect ($Q = \alpha TI$). In both devices the heat rejected must be removed through a heat sink.

The maximum efficiency of a thermoelectric material for both power generation and cooling is determined by its figure of merit (zT):

$$zT = \frac{\alpha^2 T}{\rho\kappa}$$

zT depends on α, absolute temperature (T), electrical resistivity (ρ), and thermal conductivity (κ). The best thermoelectrics are semiconductors that are so heavily doped their transport properties resemble metals.

For the past 40 years, thermoelectric generators have reliably provided power in remote terrestrial and extraterrestrial locations most notably on deep space probes such as *Voyager*. Solid-state Peltier coolers provide precise thermal management for optoelectronics and passenger seat cooling in automobiles. In the future, thermoelectric systems could harness waste heat and/or provide efficient electricity through co-generation. One key advantage of thermoelectrics is their scalability — waste heat and co-generation sources can be as small as a home water heater or as large as industrial or geothermal sources.

The Lorenz factor can vary particularly with carrier concentration. Accurate assessment of κ_e is important, as κ_l is often computed as the difference between κ and κ_e (equation (3)) using the experimental electrical conductivity. A common source of uncertainty in κ_e occurs in low-carrier-concentration materials where the Lorenz factor can be reduced by as much as 20% from the free-electron value. Additional uncertainty in κ_e arises from mixed conduction, which introduces a bipolar term into the thermal conductivity[10]. As this term is not included in the Wiedemann–Franz law, the standard computation of κ_l erroneously includes bipolar thermal conduction. This results in a perceived increase in κ_l at high temperatures for Bi_2Te_3, PbTe and others, as shown in Fig. 2a. The onset of bipolar thermal conduction occurs at nearly the same temperature as the peak in Seebeck and electrical resistivity, which are likewise due to bipolar effects.

As high zT requires high electrical conductivity but low thermal conductivity, the Wiedemann–Franz law reveals an inherent materials conflict for achieving high thermoelectric efficiency. For materials with very high electrical conductivity (metals) or very low κ_l, the Seebeck coefficient alone primarily determines zT, as can be seen in equation (4), where $(\kappa_l/\kappa_e) << 1$:

$$zT = \frac{\alpha^2/L}{1 + \frac{\kappa_l}{\kappa_e}} \quad . \tag{4}$$

LATTICE THERMAL CONDUCTIVITY

Glasses exhibit some of the lowest lattice thermal conductivities. In a glass, thermal conductivity is viewed as a random walk of energy through a lattice rather than rapid transport via phonons, and leads to the concept of a minimum thermal conductivity[22], κ_{min}. Actual glasses, however, make poor thermoelectrics because they lack the needed 'electron-crystal' properties — compared with crystalline semiconductors they have lower mobility due to increased electron scattering and lower effective masses because of broader bands. Good thermoelectrics are therefore crystalline materials that manage to scatter phonons without significantly disrupting the electrical conductivity. The heat flow is carried by a spectrum of phonons with widely varying wavelengths and mean free paths[23] (from less than 1 nm to greater than 10 μm), creating a need for phonon scattering agents at a variety of length scales.

Thermoelectrics therefore require a rather unusual material: a 'phonon-glass electron-crystal'[24]. The electron-crystal requirement stems from the fact that crystalline semiconductors have been the best at meeting the compromises required from the electronic properties (Seebeck coefficient and electrical conductivity). The phonon-glass requirement stems from the need for as low a lattice thermal conductivity as possible. Traditional thermoelectric materials have used site substitution (alloying) with isoelectronic elements to preserve a crystalline electronic structure while creating large mass contrast to disrupt the phonon path. Much of the recent excitement in the field of thermoelectrics is a result of the successful demonstration of other methods to achieve phonon-glass electron-crystal materials.

ADVANCES IN THERMOELECTRIC MATERIALS

Renewed interest in thermoelectrics is motivated by the realization that complexity at multiple length scales can lead to new mechanisms for high zT in materials. In the mid 1990s, theoretical predictions suggested that the thermoelectric efficiency could be greatly enhanced by quantum confinement of the electron charge carriers[5,25]. The electron energy bands in a quantum-confined structure are progressively narrower as the confinement increases and the dimensionality decreases. These narrow bands should produce high effective masses and therefore large Seebeck coefficients. In addition, similar sized, engineered heterostructures

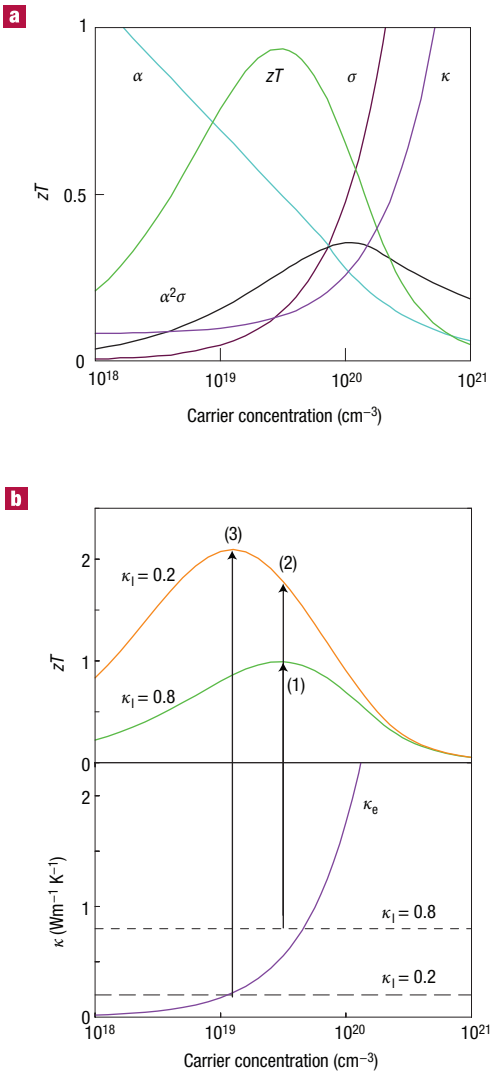

Figure 1 Optimizing zT through carrier concentration tuning. **a**, Maximizing the efficiency (zT) of a thermoelectric involves a compromise of thermal conductivity (κ; plotted on the y axis from 0 to a top value of 10 W m^{-1} K^{-1}) and Seebeck coefficient (α; 0 to 500 μV K^{-1}) with electrical conductivity (σ; 0 to 5,000 Ω^{-1}cm^{-1}). Good thermoelectric materials are typically heavily doped semiconductors with a carrier concentration between 10^{19} and 10^{21} carriers per cm^3. The thermoelectric power factor $\alpha^2\sigma$ maximizes at higher carrier concentration than zT. The difference between the peak in $\alpha^2\sigma$ and zT is greater for the newer lower-κ_l materials. Trends shown were modelled from Bi_2Te_3, based on empirical data in ref. 78. **b**, Reducing the lattice thermal conductivity leads to a two-fold benefit for the thermoelectric figure of merit. An optimized zT of 0.8 is shown at point (1) for a model system (Bi_2Te_3) with a κ_l of 0.8 Wm^{-1} K^{-1} and κ_e that is a function of the carrier concentration (purple). Reducing κ_l to 0.2 Wm^{-1} K^{-1} directly increases the zT to point (2). Additionally, lowering the thermal conductivity allows the carrier concentration to be reoptimized (reduced), leading to both a decrease in κ_e and a larger Seebeck coefficient. The reoptimized zT is shown at point (3).

may decouple the Seebeck coefficient and electrical conductivity due to electron filtering[26] that could result in high zT. Even though a high-ZT device based on these principles has yet to be demonstrated, these predictions have stimulated a new wave of interest in complex thermoelectric materials. Vital to this rebirth has been interdisciplinary collaborations: research in thermoelectrics

Box 2 State-of-the-art high-zT materials

To best assess the recent progress and prospects in thermoelectric materials, the decades of research and development of the established state-of-the-art materials should also be considered. By far the most widely used thermoelectric materials are alloys of Bi_2Te_3 and Sb_2Te_3. For near-room-temperature applications, such as refrigeration and waste heat recovery up to 200 °C, Bi_2Te_3 alloys have been proved to possess the greatest figure of merit for both n- and p-type thermoelectric systems. Bi_2Te_3 was first investigated as a material of great thermoelectric promise in the 1950s[12,16–18,84]. It was quickly realized that alloying with Sb_2Te_3 and Bi_2Se_3 allowed for the fine tuning of the carrier concentration alongside a reduction in lattice thermal conductivity. The most commonly studied p-type compositions are near $(Sb_{0.8}Bi_{0.2})_2Te_3$ whereas n-type compositions are close to $Bi_2(Te_{0.8}Se_{0.2})_3$. The electronic transport properties and detailed defect chemistry (which controls the dopant concentration) of these alloys are now well understood thanks to extensive studies of single crystal and polycrystalline material[85,86]. Peak zT values for these materials are typically in the range of 0.8 to 1.1 with p-type materials achieving the highest values (Fig. B2a,b). By adjusting the carrier concentration zT can be optimized to peak at different temperatures, enabling the tuning of the materials for specific applications such as cooling or power generation[87]. This effect is demonstrated in Fig. B2c for PbTe.

For mid-temperature power generation (500–900 K), materials based on group-IV tellurides are typically used, such as PbTe, GeTe or SnTe[12,17,18,81,88]. The peak zT in optimized n-type material is about 0.8. Again, a tuning of the carrier concentration will alter the temperature where zT peaks. Alloys, particularly with $AgSbTe_2$, have led to several reports of $zT > 1$ for both n-type and p-type materials[73,89,90]. Only the p-type alloy $(GeTe)_{0.85}(AgSbTe_2)_{0.15}$, commonly referred to as TAGS, with a maximum zT greater than 1.2 (ref. 69), has been successfully used in long-life thermoelectric generators. With the advent of modern microstructural and chemical analysis techniques, such materials are being reinvestigated with great promise (see section on nanomaterials).

Successful, high-temperature (>900 K) thermoelectric generators have typically used silicon–germanium alloys for both n- and p-type legs. The zT of these materials is fairly low, particularly for the p-type material (Fig. B2b) because of the relatively high lattice thermal conductivity of the diamond structure.

For cooling below room temperature, alloys of BiSb have been used in the n-type legs, coupled with p-type legs of $(Bi,Sb)_2(Te,Se)_3$ (refs 91,92). The poor mechanical properties of BiSb leave much room for improved low-temperature materials.

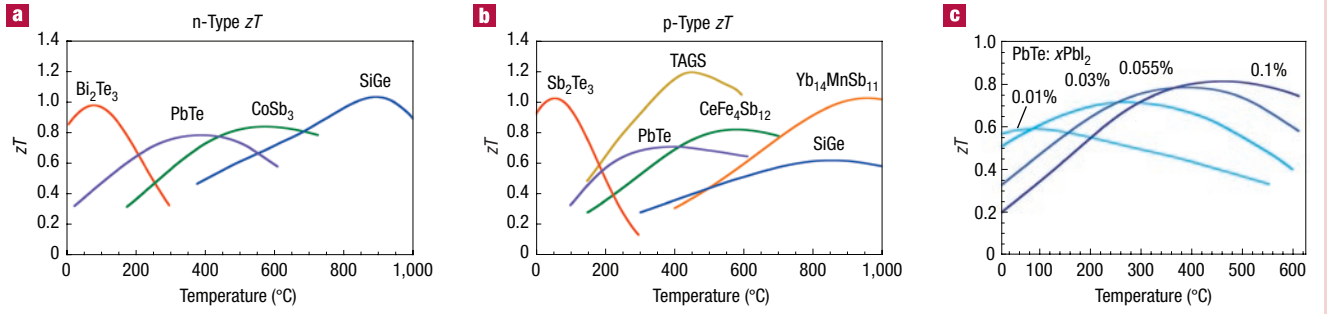

Figure B2 Figure-of-merit zT of state-of-the-art commercial materials and those used or being developed by NASA for thermoelectric power generation. **a**, p-type and **b**, n-type. Most of these materials are complex alloys with dopants; approximate compositions are shown. **c**, Altering the dopant concentration changes not only the peak zT but also the temperature where the peak occurs. As the dopant concentration in n-type PbTe increases (darker blue lines indicate higher doping) the zT peak increases in temperature. Commercial alloys of Bi_2Te_3 and Sb_2Te_3 from Marlow Industries, unpublished data; doped PbTe, ref. 88; skutterudite alloys of $CoSb_3$ and $CeFe_4Sb_{12}$ from JPL, Caltech unpublished data; TAGS, ref. 69; SiGe (doped $Si_{0.8}Ge_{0.2}$), ref. 82; and $Yb_{14}MnSb_{11}$, ref. 45.

requires an understanding of solid-state chemistry, high-temperature electronic and thermal transport measurements, and the underlying solid-state physics. These collaborations have led to a more complete understanding of the origin of good thermoelectric properties.

There are unifying characteristics in recently identified high-zT materials that can provide guidance in the successful search for new materials. One common feature of the thermoelectrics recently discovered with zT>1 is that most have lattice thermal conductivities that are lower than the present commercial materials. Thus the general achievement is that we are getting closer to a 'phonon glass' while maintaining the 'electron crystal.' These reduced lattice thermal conductivities are achieved through phonon scattering across various length scales as discussed above. A reduced lattice thermal conductivity directly improves the thermoelectric efficiency, zT, (equation (4)) and additionally allows re-optimization of the carrier concentration for additional zT improvement (Fig. 1b).

There are three general strategies to reduce lattice thermal conductivity that have been successfully used. The first is to scatter phonons within the unit cell by creating rattling structures or point defects such as interstitials, vacancies or by alloying[27]. The second strategy is to use complex crystal structures to separate the electron-crystal from the phonon-glass. Here the goal is to be able to achieve a phonon glass without disrupting the crystallinity of the electron-transport region. A third strategy is to scatter phonons at interfaces, leading to the use of multiphase composites mixed on the nanometre scale[5]. These nanostructured materials can be formed as thin-film superlattices or as intimately mixed composite structures.

COMPLEXITY THROUGH DISORDER IN THE UNIT CELL

There is a long history of using atomic disorder to reduce the lattice thermal conductivity in thermoelectrics (Box 2). Early work by

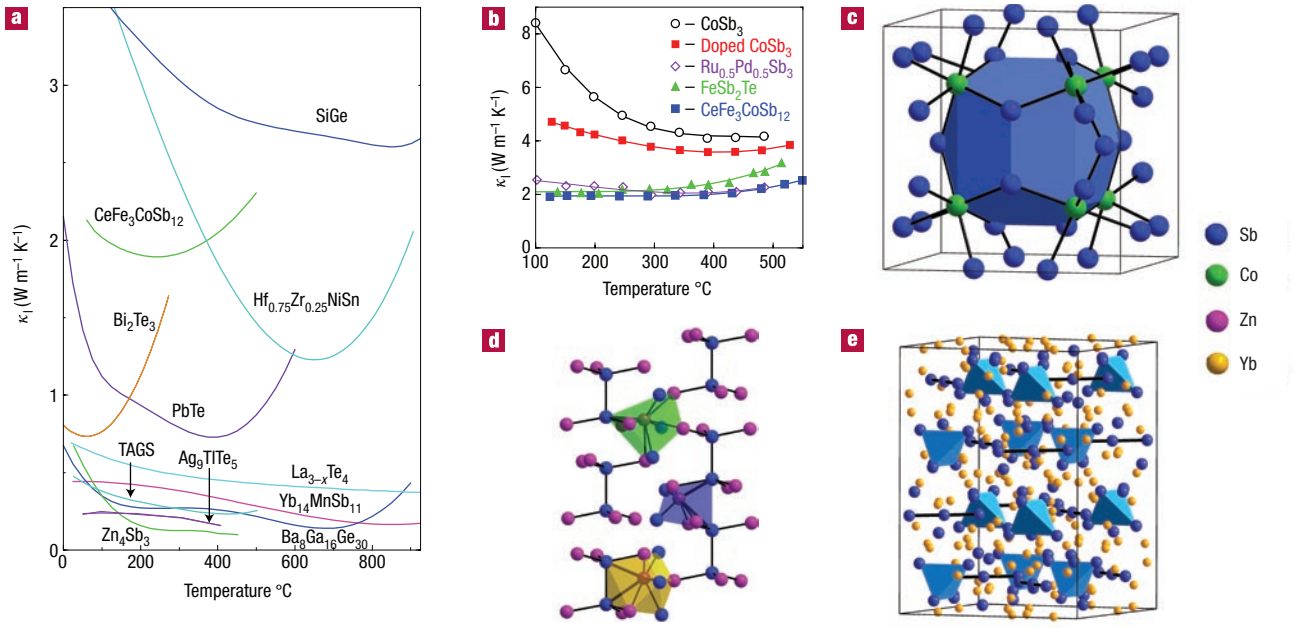

Figure 2 Complex crystal structures that yield low lattice thermal conductivity. **a**, Extremely low thermal conductivities are found in the recently identified complex material systems (such as $Yb_{14}MnSb_{11}$, ref. 45; $CeFe_3CoSb_{12}$, ref. 34; $Ba_8Ga_{16}Ge_{30}$, ref. 79; and Zn_4Sb_3, ref. 80; Ag_9TlTe_5, ref. 40; and $La_{3-x}Te_4$, Caltech unpublished data) compared with most state-of-the-art thermoelectric alloys (Bi_2Te_3, Caltech unpublished data; PbTe, ref. 81; TAGS, ref. 69; SiGe, ref. 82 or the half-Heusler alloy $Hf_{0.75}Zr_{0.25}NiSn$, ref. 83). **b**, The high thermal conductivity of $CoSb_3$ is lowered when the electrical conductivity is optimized by doping (doped $CoSb_3$). The thermal conductivity is further lowered by alloying on the Co ($Ru_{0.5}Pd_{0.5}Sb_3$) or Sb ($FeSb_2Te$) sites or by filling the void spaces ($CeFe_3CoSb_{12}$) (ref. 34). **c**, The skutterudite structure is composed of tilted octahedra of $CoSb_3$ creating large void spaces shown in blue. **d**, The room-temperature structure of Zn_4Sb_3 has a crystalline Sb sublattice (blue) and highly disordered Zn sublattice containing a variety of interstitial sites (in polyhedra) along with the primary sites (purple). **e**, The complexity of the $Yb_{14}MnSb_{11}$ unit cell is illustrated, with $[Sb_3]^{7-}$ trimers, $[MnSb_4]^{9-}$ tetrahedra, and isolated Sb anions. The Zintl formalism describes these units as covalently bound with electrons donated from the ionic Yb^{2+} sublattice (yellow).

Wright discusses how alloying Bi_2Te_3 with other isoelectronic cations and anions does not reduce the electrical conductivity but lowers the thermal conductivity[28]. Alloying the binary tellurides (Bi_2Te_3, Sb_2Te_3, PbTe and GeTe) continues to be an active area of research[29–32]. Many of the recent high-zT thermoelectric materials similarly achieve a reduced lattice thermal conductivity through disorder within the unit cell. This disorder is achieved through interstitial sites, partial occupancies, or rattling atoms in addition to the disorder inherent in the alloying used in the state-of-the-art materials. For example, rare-earth chalcogenides[18] with the Th_3P_4 structure (for example $La_{3-x}Te_4$) have a relatively low lattice thermal conductivity (Fig. 2a) presumably due to the large number of random vacancies (x in $La_{3-x}Te_4$). As phonon scattering by alloying depends on the mass ratio of the alloy constituents, it can be expected that random vacancies are ideal scattering sites.

The potential to reduce thermal conductivity through disorder within the unit cell is particularly large in structures containing void spaces. One class of such materials are clathrates[8], which contain large cages that are filled with rattling atoms. Likewise, skutterudites[7] such as $CoSb_3$, contain corner-sharing $CoSb_6$ octahedra, which can be viewed as a distorted variant of the ReO_3 structure. These tilted octahedra create void spaces that may be filled with rattling atoms, as shown in Fig. 2c with a blue polyhedron[33].

For skutterudites containing elements with low electronegativity differences such as $CoSb_3$ and $IrSb_3$, there is a high degree of covalent bonding, enabling high carrier mobilities and therefore good electron-crystal properties. However, this strong bonding and simple order leads to high lattice thermal conductivities. Thus, the challenge with skutterudites has been the reduction of the lattice thermal conductivity. Doping $CoSb_3$ to carrier concentrations that optimize zT adds enough carriers to substantially reduce thermal conductivity[34] through electron–phonon interactions (Fig. 2b). Further reductions can be obtained by alloying either on the transition metal or the antimony site.

Filling the large void spaces with rare-earth or other heavy atoms further reduces the lattice thermal conductivity[35]. A clear correlation has been found with the size and vibrational motion of the filling atom and the thermal conductivity leading to zT values as high as 1 (refs 8,13). Partial filling establishes a random alloy mixture of filling atoms and vacancies enabling effective point-defect scattering as discussed previously. In addition, the large space for the filling atom in skutterudites and clathrates can establish soft phonon modes and local or 'rattling' modes that lower lattice thermal conductivity.

Filling these voids with ions adds additional electrons that require compensating cations elsewhere in the structure for charge balance, creating an additional source of lattice disorder. For the case of $CoSb_3$, Fe^{2+} frequently is used to substitute Co^{3+}. An additional benefit of this partial filling is that the free-carrier concentration may be tuned by moving the composition slightly off the charge-balanced composition. Similar charge-balance arguments apply to the clathrates, where filling requires replacing group 14 (Si, Ge) with group 13 (Al, Ga) atoms.

COMPLEX UNIT CELLS

Low thermal conductivity is generally associated with crystals containing large, complex unit cells. The half-Heusler alloys[8] have a simple, cubic structure with high lattice thermal conductivity ($Hf_{0.75}Zr_{0.25}NiSb$ in Fig. 2a) that limits the zT. Thus complex crystal structures are good places to look for improved materials. A good

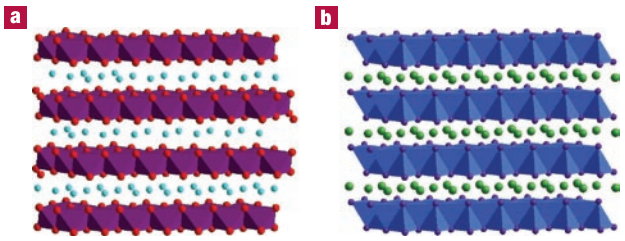

Figure 3 Substructure approach used to separate the electron-crystal and phonon-glass attributes of a thermoelectric. **a**, Na_xCoO_2 and **b**, $Ca_xYb_{1-x}Zn_2Sb_2$ structures both contain ordered layers (polyhedra) separated by disordered cation monolayers, creating electron-crystal phonon-glass structures.

example of a complex variant of Bi_2Te_3 is $CsBi_4Te_6$, which has a somewhat lower lattice thermal conductivity than Bi_2Te_3 that has been ascribed to the added complexity of the Cs layers and the few Bi–Bi bonds in $CsBi_4Te_6$ not found in Bi_2Te_3. These Bi–Bi bonds lower the bandgap compared with Bi_2Te_3, dropping the maximum zT of $CsBi_4Te_6$ below room temperature with a maximum zT of 0.8 (refs 8,36). Like Bi_2Te_3, the layering in $CsBi_4Te_6$ leads to an anisotropic effective mass that can improve the Seebeck coefficient with only minor detriment to the mobility[8]. Many ordered MTe/Bi_2Te_3-type variants (M = Ge, Sn or Pb)[37,38] are known, making up a large homologous series of compounds[39], but to date $zT < 0.6$ is found in most reports. As many of these materials have low lattice thermal conductivities but have not yet been doped to appropriate carrier concentrations, much remains to be done with complex tellurides.

Low lattice thermal conductivities are also seen in the thallium-based thermoelectric materials such as Ag_9TlTe_5 (ref. 40) and Tl_9BiTe_6 (ref. 41). Although these materials do have complex unit cells, there is clearly something unique about the thallium chemistry that leads to low thermal conductivity (0.23 W m^{-1} K^{-1} at room temperature[40]). One possible explanation is extremely soft thallium bonding, which can also be observed in the low elastic modulus these materials exhibit.

The remarkably high zT in Zn_4Sb_3 arises from the exceptionally low, glass-like thermal conductivity (Fig. 2a). In the room-temperature phase, about 20% of the Zn atoms are on three crystallographically distinct interstitial sites as shown in Fig. 2d. These interstitials are accompanied by significant local lattice distortions[42] and are highly dynamic, with Zn diffusion rates almost as high as that of superionic conductors[43]. Pair distribution function (PDF) analysis[44] of X-ray and neutron diffraction data shows that there is local ordering of the Zn interstitials into nanoscale domains. Thus, the low thermal conductivity of Zn_4Sb_3 arises from disorder at multiple length scales, from high levels of interstitials and corresponding local structural distortions and from domains of interstitial ordering. Within the unit cell, Zn interstitials create a phonon glass, whereas the more ordered Sb framework provides the electron-crystal component.

One common characteristic of nearly all good thermoelectric materials is valence balance — charge balance of the chemical valences of all atoms. Whether the bonding is ionic or covalent, valence balance enables the separation of electron energy bands needed to form a bandgap. Complex Zintl compounds have recently emerged as a new class of thermoelectrics[9] because they can form quite complex crystal structures. A Zintl compound contains a valence-balanced combination of both ionically and covalently bonded atoms. The mostly ionic cations donate electrons to the covalently bound anionic species. The covalent bonding allows higher mobility of the charge-carrier species than that found in purely ionic materials. The combination of the bonding types leads to complex structures with the possibility of multiple structural units in the same structure. One example is $Yb_{14}MnSb_{11}$ (refs 45,46), which contains $[MnSb_4]^{9-}$ tetrahedra, polyatomic $[Sb_3]^{7-}$ anions, as well as isolated Sb^{3-} anions and Yb^{2+} cations (Fig. 2e). This structural complexity, despite the crystalline order, enables extremely low lattice thermal conductivity (0.4 W m^{-1} K^{-1} at room temperature; Fig. 2a). Combined with large Seebeck coefficient and high electrical conductivity, $Yb_{14}MnSb_{11}$ results in a zT of ~1.0 at 900 °C. This zT is nearly twice that of p-type SiGe used in NASA spacecraft and has led to rapid acceptance of $Yb_{14}MnSb_{11}$ into NASA programmes for development of future thermoelectric generators. The complexity of Zintl structures also makes them ideal materials for using a substructure approach.

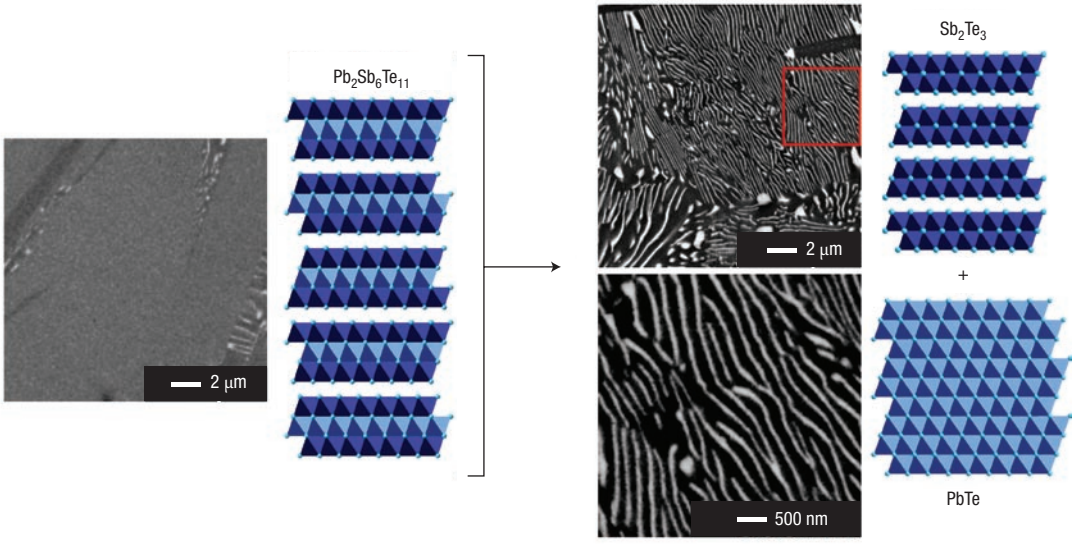

Figure 4 Nanostructured thermoelectrics may be formed by the solid-state partitioning of a precursor phase. The metastable $Pb_2Sb_6Te_{11}$ phase (left) will spontaneously assemble into lamellae of Sb_2Te_3 and PbTe (ref. 76; right). These domains are visible with backscattering scanning electron microscopy, with the dark regions corresponding to Sb_2Te_3 and the light regions to PbTe. Electron backscattering diffraction reveals that the lamellae are oriented with coherent interfaces, shown schematically (right).

Box 3 Thermoelectric measurements

Many materials have been reported with $zT > 1.5$ but few have been confirmed by others, and no devices have been assembled that show the efficiency expected from such high-zT materials. This is due to the complexity of fabricating devices, measurement uncertainty and materials complications.

The inherent difficulty in thermoelectrics is that direct efficiency measurements require nearly as much complexity as building an entire device. Thus practical assessment of the thermoelectric figure of merit typically relies on measuring the individual contributing material properties (σ, α and κ). Measurements of the thermoelectric properties are conceptually simple but results can vary considerably, particularly above room temperature where thermal gradients in the measurement system add to systematic inaccuracies. As a typical zT measurement above room temperature requires the measurement of σ, α and κ (from the density, heat capacity, C_p, and thermal diffusivity, D) each with uncertainty of 5% to 20%, the uncertainty in zT from

$$\frac{\Delta z}{z} = 2\frac{\Delta \alpha}{\alpha} + \frac{\Delta \sigma}{\sigma} + \frac{\Delta C_p}{C_p} + \frac{\Delta D}{D}$$

could easily reach 50%. Accuracy is particularly important for the Seebeck coefficient because it is squared in the calculation of zT and there are few standards with which to calibrate systems. In addition, a variety of geometric terms are required in these calculations (density, thickness and coefficient of thermal expansion[79]).

The sensitivity of the materials themselves to impurities and dopant concentrations further complicates measurements. This is because of the strong dependence of conductivity and to a lesser extent Seebeck coefficient on carrier concentration (Fig. 1a). Small inhomogeneities can result in large variations in thermoelectric properties within a sample[71], making repeatability and combining results of different measurements difficult. For example, combining Seebeck and resistivity on one sample or set of contacts and thermal conductivity on another could lead to spurious results. Likewise, reliable property values are particularly difficult to obtain when sublimation, microstructural evolution, electrochemical reactions and phase transitions are present. Thus, even the act of measuring a sample at high temperatures can alter its properties

The hallmarks of trustworthy measurements are slow, physical trends in properties. Typical materials (Box 2) show a linear or concave downward trend in Seebeck coefficient with temperature and only slow variation with chemical doping. Abrupt transitions to high-zT materials (as a function of temperature or composition) are unlikely. Thin-film samples are particularly difficult to measure. Electrical conductivity often depends critically on the perceived thickness of the conducting layer — if the substrate or quantum-well walls become conducting at any time, it can lead to an erroneously high electrical conductivity estimate of the film. Thermal conductivity and the Seebeck effect likewise depend significantly on the assumption that the substrate and insulating superlattice layers do not change with processing, atmosphere, or temperature. One should be encouraged by results of $zT > 1$ but remain wary of the uncertainties involved to avoid pathological optimism.

SUBSTRUCTURE APPROACH

One method for circumventing the inherent materials conflict of a phonon-glass with electron-crystal properties is to imagine a complex material with distinct regions providing different functions. Such a substructure approach would be analogous to the enabling features that led to high-T_c superconductivity in copper oxides. In these materials, the free charge carriers are confined to planar Cu–O sheets that are separated by insulating oxide layers. Precise tuning of the carrier concentration is essential for superconductivity. This is enabled by the insulating layers acting as a 'charge reservoir'[47] that houses dopant atoms that donate charge carriers to the Cu–O sheets. The separation of the doping regions from the conduction regions keeps the charge carriers sufficiently screened from the dopant atoms so as not to trap carriers, which would lead to a low mobility, hopping conduction mechanism rather than superconductivity.

Likewise, the ideal thermoelectric material would have regions of the structure composed of a high-mobility semiconductor that provides the electron-crystal electronic structure, interwoven with a phonon-glass. The phonon-glass region would be ideal for housing dopants and disordered structures without disrupting the carrier mobility in the electron-crystal region, much like the charge-reservoir region in high-T_c superconductors. The electron crystal regions will need to be thin, on the nanometre or ångström scale, so that phonons with a short mean free path are scattered by the phonon-glass region. Such thin, low-dimensional electron-transport regions might also be able to take advantage of quantum confinement and/or electron filtering to enhance the Seebeck coefficient. Skutterudites and clathrates represent a 0-dimensional version of the substructure approach, with isolated rattlers in an electron-crystal matrix.

The thermoelectric cobaltite oxides (Na_xCoO_2 and others such as those based on the Ca–Co–O system) may likewise be described using a substructure approach[14,48,49]. The Co–O layers form metallic layers separated by insulating, disordered layers with partial occupancies (Fig. 3a). Oxides typically have low mobilities and high lattice thermal conductivity, due to the high electronegativity of oxygen and the strong bonding of light atoms, respectively. These properties give oxides a distinct disadvantage for thermoelectric materials. The relatively large Seebeck values obtained in these systems has been attributed to spin-induced entropy[50]. The success of the cobaltite structures as thermoelectric materials may be an early example of how the substructure approach overcomes these disadvantages. The study of oxide thermoelectrics benefits greatly from the variety of structures and synthetic techniques known for oxides, as well as our understanding of oxide structure–property relationships.

Zintl compounds may be more appropriate for substructure-based thermoelectrics due to the nature of their bonding. The covalently bound anion substructures can adopt a variety of topologies — from 0-dimensional isolated single ions, dimers and polyatomic anions to extended one-, two- and three-dimensional chains, planes and nets[9]. This covalently bound substructure enables high carrier mobilities whereas the ionic cation substructure is amenable to doping and site disorder without disrupting the covalent network. The valence-balanced bonding in these materials frequently leads to bandgaps that are of a suitable size for thermoelectric applications.

The substructure approach is clearly seen in the Zintl compound $Ca_xYb_{1-x}Zn_2Sb_2$ (ref. 51), whose structure is similar to Na_xCoO_2, with sheets of disordered cations between layers of covalently bound Zn–Sb (Fig. 3b). $Ca_xYb_{1-x}Zn_2Sb_2$ demonstrates the fine-tuning ability in the ionic layer concomitant with a modest reduction in lattice thermal conductivity due to alloying of Yb and Ca. The Ca^{2+} is slightly more electropositive than Yb^{2+}, which enables a gradual changing of the carrier concentration as the Yb:Ca ratio is changed. This doping produces disorder on the cation substructure

Box 4 Thermoelectric efficiency

The efficiency of a thermoelectric device depends on factors other than the maximum zT of a material. This is primarily due to the temperature dependence of all the materials properties (α, σ, κ) that make up $zT(T)$. For example, even for state-of-the-art Bi_2Te_3, which has a peak zT value of 1.1, the effective device ZT is only about 0.7 based on the overall performance of the device as a cooler or power generator.

Here we use ZT (upper case) to distinguish the device figure of merit from lower-case $zT = \alpha^2\sigma/\kappa$, the material's figure of merit[10]. For a Peltier cooler the device ZT is most easily measured from the maximum temperature drop obtained (ΔT_{max}).

$$\Delta T_{max} = \frac{ZT_c^2}{2} \quad .$$

For a generator, the maximum efficiency (η) is used to determine ZT:

$$\eta = \frac{\Delta T}{T_h} \cdot \frac{\sqrt{1+ZT}-1}{\sqrt{1+ZT}+\frac{T_c}{T_h}} \quad .$$

Like all heat engines, the maximum power-generation efficiency of a thermoelectric generator is thermodynamically limited by the Carnot efficiency ($\Delta T/T_h$). If temperature is assumed to be independent and n-type and p-type thermoelectric properties are matched (α, σ and κ), (an unrealistic approximation in many cases) the maximum device efficiency is given by the above equation with $Z = z$.

To maximize efficiency across a large temperature drop, it is imperative to maximize the device ZT, and not just a peak materials zT. One method to achieve this is to tune the material to provide a large average $zT(T)$ in the temperature range of interest. For example, the peak zT in PbTe may be tuned from 300 °C to 600 °C (see Fig. B2c). For large temperature differences (needed to achieve high Carnot efficiency) segmenting with different materials that have peak zT at different temperatures (see Fig. B2a,b) will improve device ZT (ref. 93). Functionally graded materials can also be used to continuously tune zT instead of discrete segmenting[94].

For such large ΔT applications the device ZT can be significantly smaller than even the average zT due to thermoelectric incompatibility. Across a large ΔT, the electrical current required for highest-efficiency operation changes as the materials properties change with temperature or segment[95]. This imposes an additional materials requirement: the thermoelectric compatibility factors ($s = (\sqrt{(1+zT)} \pm 1)/\alpha T$) with – for power generation[96] or + for cooling[97]) must be similar. For high efficiency, this term needs to be within about a factor of two across the different temperature ranges[95]. A compelling example of the need for compatibility matching is segmenting TAGS with SiGe. The compatibility is so poor between these materials that replacing SiGe with $Yb_{14}MnSb_{11}$ quadruples the device efficiency increase for adding the additional high-temperature segment[45].

but not the conducting anion substructure such that the bandgap and carrier mobility is unchanged. The disorder on the cation substructure does indeed lower the lattice thermal conductivity producing a modest increase in zT. However, the relatively simple structure of $Ca_xYb_{1-x}Zn_2Sb_2$ leads to relatively high lattice thermal conductivities (~1.5 W m^{-1} K^{-1}) — suggesting further methods to reduce the conductivity, such as nanostructuring, would lead to an improved material.

Given the broad range of phonons involved in heat transport, a substructure approach may only be one component in a high-performance thermoelectric material. Long-wavelength phonons require disorder on longer length-scales, leading to a need for hierarchical complexity. Combining a substructure approach with nanostructuring seems to be the most promising method of achieving a high-Seebeck, high-conductivity material that manages to scatter phonons at all length scales.

COMPLEX NANOSTRUCTURED MATERIALS

Much of the recent interest in thermoelectrics stems from theoretical and experimental evidence of greatly enhanced zT in nanostructured thin-films and wires due to enhanced Seebeck and reduced thermal conductivity[5]. Reduced thermal conductivity in thin-film superlattices was investigated in the 1980s[52], but has only recently been applied to enhanced thermoelectric materials. Recent efforts[53–55] on Bi_2Te_3-Sb_2Te_3 and PbTe–PbSe films and Si nanowires[56,57] have shown how phonon scattering can reduce lattice thermal conductivity to near κ_{min} values[22,58] (0.2–0.5 W m^{-1} K^{-1}). Thin films containing randomly embedded quantum dots likewise achieve exceptionally low lattice thermal conductivities[59,60]. Very high zT values (>2) have been reported in thin films but the difficulty of measurements makes them a challenge to reproduce in independent labs (Box 3). It is clear however that nanostructured thin-films and wires do exhibit lattice thermal conductivities near (or even below[61]) κ_{min}, which results in higher material zT, but improvements of electrical and thermal contacts to these materials in a device are needed before higher device ZT (Box 4) is achieved.

The use of bulk (mm^3) nanostructured materials would avoid detrimental electrical and thermal losses and use the existing fabrication routes. The challenge for any nanostructured bulk material system is electron scattering at interfaces between randomly oriented grains leading to a concurrent reduction of both the electrical and thermal conductivities[27]. The effect of grain-boundary scattering in a silicon–germanium system has been extensively studied, as the system possesses excellent electron-crystal properties but very high thermal conductivities. In 1981, the synthesis of polycrystalline silicon germanium alloys were described, and the decrease in thermal conductivity with smaller grain size was tracked[62]. Compared with single crystals of SiGe alloys, polycrystalline materials with grains on the order of 1 μm show an enhanced zT. However, later experiments on materials with grains between 1–100 μm found that the increased phonon scattering was offset by the decrease in electrical conductivity[63]. Nevertheless, recent work suggests that truly nanostructured SiGe enhances zT (ref. 5).

The results on epitaxial thin-films suggests that the ideal nanostructured material would have thermodynamically stable, coherent, epitaxy-like, interfaces between the constituent phases to prevent grain-boundary scattering of electrons. Thus, a promising route to nanostructured bulk thermoelectric materials relies on the spontaneous partitioning of a precursor phase into thermodynamically stable phases[64]. The growth and characterization of such composite microsctructures have been studied in metals for decades because of their ability to greatly improve mechanical strength. The use of microstructure to reduce thermal conductivity in thermoelectrics, dates to the 1960s[65]. For example, crystals pulled from an InSb–Sb eutectic alloy, which forms rods of Sb as

thin as 4 μm in an InSb matrix, shows a clear decrease in thermal conductivity with smaller rod diameters, in both parallel and perpendicular directions[66]. Additionally, no major decrease in electrical conductivity or Seebeck coefficient was observed. In a similar manner, several eutectics form from two thermoelectrics form such as rock salt–tetradymite (for example, PbTe–Sb_2Te_3) revealing a variety of layered and dendritic microstructures[64,67]. A fundamental limitation of such an approach is that rapid diffusion in the liquid phase leads to coarse microstructures[67,68].

Microstructural complexity may explain why $(AgSbTe_2)_{0.15}(GeTe)_{0.85}$ (TAGS) and $(AgSbTe_2)_x(PbTe)_{1-x}$ (LAST), first studied in the 1950s, have remained some of the materials having highest known zT. Originally believed to be a true solid solution with the rock-salt structure, recent interest has focused on the nanoscale microstructure and even phase separation that exists in these and related alloy compositions. From early on it was predicted that lattice strain in TAGS could explain the low lattice thermal conductivities of 0.3 W m^{-1} K^{-1} (ref. 69). Recent work points to the presence of twin-boundary defects in TAGS as an additional source of phonon scattering[70]. Inhomogeneities on various length scales[69] have been found in LAST alloys, which may be associated with the reports of high zT; however, this also makes reproducibility a challenge. In LAST, Ag–Sb rich nanoparticles 1–10 nm in size as well as larger micrometre-sized features precipitate from the bulk[71–73]. The nanoparticles are oriented within the rock-salt crystal with coherent interfaces, therefore electronic conductivity is not significantly reduced. Conversely, the large density difference between the different regions leads to interfacial scattering of the phonons, reducing the thermal conductivity. Through these mechanisms, thermal conductivities of the order of 0.5 W m^{-1} K^{-1} at 700 K have been observed. A variety of other materials have been formed that have oriented nanoparticle inclusions in a PbTe matrix[31,32,74].

As the thermoelectric properties of nanostructured materials should depend on the size and morphology of the microstructural features, the materials science of microstructural engineering should become increasingly important in the development of thermoelectric nanomaterials. Our group has focused on the partitioning of quenched, metastable phases that then transform into two phases during a controlled process[75,76]. By restricting the partitioning to solid-state diffusion at low temperatures, the resulting microstructures are quite fine. Figure 4 shows a sample of $Pb_2Sb_6Te_{11}$ after quenching and the microstructure that results on annealing at 400 °C. A lamellar spacing of 360 nm is observed, corresponding to 80-nm PbTe and 280-nm Sb_2Te_3 layer thicknesses. The lamellar spacing can be controlled from below 200 nm to several micrometres. One appealing aspect of this lamellar growth is that the low lattice mismatch between the PbTe (111) and Sb_2Te_3 (001) planes leads to coherent interfaces between the lamellae. Controlled partitioning of a precursor solid can also be done from a glass, as in the case of the alloy glass $(GeSe_2)_{70}(Sb_2Te_3)_{20}(GeTe)_{10}$, which devitrifies to fine lamellae of $GeSe_2$ and $GeSb_4Te_7$ (ref. 77). The numerous possibilities for controlling such reactions will introduce complexity at multiple length scales to thermoelectric materials engineering.

CONCLUDING REMARKS

The conflicting material properties required to produce a high-efficiency (phonon-glass electron-crystal) thermoelectric material have challenged investigators over the past 50 years. Recently, the field has undergone a renaissance with the discovery of complex high-efficiency materials that manage to decouple these properties. A diverse array of new approaches, from complexity within the unit cell to nanostructured bulk and thin-film materials, have all led to high-efficiency materials. Given the complexity of these systems, all of these approaches benefit from collaborations between chemists, physicists and materials scientists. The global need for sustainable energy coupled with the recent advances in thermoelectrics inspires a growing excitement in this field.

doi:10.1038/nmat2090

References

1. Rowe, D. M. (ed.) *CRC Handbook of Thermoelectrics* (CRC, Boca Raton, 1995).
2. Matsubara, K. in *International Conference on Thermoelectrics* 418–423 (2002).
3. DiSalvo, F. J. Thermoelectric cooling and power generation. *Science* **285,** 703–706 (1999).
4. Rowe, D. M. (ed.) *CRC Handbook of Thermoelectrics: Macro to Nano* (CRC, Boca Raton, 2005).
5. Dresselhaus, M. S. *et al.* New directions for low-dimensional thermoelectric materials. *Adv. Mater.* **19,** 1043–1053 (2007).
6. Chen, G., Dresselhaus, M. S., Dresselhaus, G., Fleurial, J. P. & Caillat, T. Recent developments in thermoelectric materials. *Int. Mater. Rev.* **48,** 45–66 (2003).
7. Uher, C. in *Thermoelectric Materials Research I* (ed. Tritt, T.) 139–253 (Semiconductors and Semimetals Series 69, Elsevier, 2001).
8. Nolas, G. S., Poon, J. & Kanatzidis, M. Recent developments in bulk thermoelectric materials. *Mater. Res. Soc. Bull.* **31,** 199–205 (2006).
9. Kauzlarich, S. M., Brown, S. R. & Snyder, G. J. Zintl phases for thermoelectric devices. *Dalton Trans.* 2099–2107 (2007).
10. Goldsmid, H. J. *Applications of Thermoelectricity* (Methuen, London, 1960).
11. Tritt, T. M. (ed.) *Recent Trends in Thermoelectric Materials Research* (Academic, San Diego, 2001).
12. Heikes, R. R. & Ure, R. W. *Thermoelectricity: Science and Engineering* (Interscience, New York, 1961).
13. Sales, B. C. Electron crystals and phonon glasses: a new path to improved thermoelectric materials. *Mater. Res. Soc. Bull.* **23,** 15–21 (1998).
14. Koumoto, K., Terasaki, I. & Funahashi, R. Complex oxide materials for potential thermoelectric applications. *Mater. Res. Soc. Bull.* **31,** 206–210 (2006).
15. Mahan, G. D. in *Solid State Physics* Vol. 51 (eds Ehrenreich, H. & Spaepen, F.) 81–157 (Elsevier, 1998).
16. Rosi, F. D. Thermoelectricity and thermoelectric power generation. *Solid-State Electron.* **11,** 833–848 (1968).
17. Rosi, F. D., Hockings, E. F. & Lindenblad, N. E. Semiconducting materials for thermoelectric power generation. *RCA Rev.* **22,** 82–121 (1961).
18. Wood, C. Materials for thermoelectric energy-conversion. *Rep. Prog. Phys.* **51,** 459–539 (1988).
19. Cutler, M., Leavy, J. F. & Fitzpatrick, R. L. Electronic transport in semimetallic cerium sulfide. *Phys. Rev.* **133,** A1143–A1152 (1964).
20. Bhandari, C. M. & Rowe, D. M. in *CRC Handbook of Thermoelectrics* (ed. Rowe, D. M.) Ch. 5, 43–53 (CRC, Boca Raton, 1995).
21. Snyder, G. J., Caillat, T. & Fleurial, J.-P. Thermoelectric transport and magnetic properties of the polaron semiconductor $Fe_xCr_{3-x}Se_4$. *Phys. Rev. B* **62,** 10185 (2000).
22. Slack, G. A. (ed.) *Solid State Physics* (Academic Press, New York, 1979).
23. Dames, C. & Chen, G. in *Thermoelectrics Handbook Macro to Nano* (ed. Rowe, D. M.) Ch. 42 (CRC, Boca Raton, 2006).
24. Slack, G. A. in *CRC Handbook of Thermoelectrics* (ed. Rowe, M.) 407–440 (CRC, Boca Raton, 1995).
25. Hicks, L. D. & Dresselhaus, M. S. Effect of quantum-well structures on the thermoelectric figure of merit. *Phys. Rev. B* **47,** 12727–12731 (1993).
26. Zide, J. M. O. *et al.* Demonstration of electron filtering to increase the Seebeck coefficient in $In_{0.53}Ga_{0.47}As/In_{0.53}Ga_{0.28}Al_{0.19}As$ superlattices. *Phys. Rev. B* **74,** 205335 (2006).
27. Bhandari, C. M. in *CRC Handbook of Thermoelectrics* (ed. Rowe, D. M.) 55–65 (CRC, Boca Raton, 1995).
28. Wright, D. A. Thermoelectric properties of bismuth telluride and its alloys. *Nature* **181,** 834–834 (1958).
29. Kusano, D. & Hori, Y. Thermoelectric properties of p-type $(Bi_2Te_3)(0.2)$ $(Sb_2Te_3)(0.8)$ thermoelectric material doped with PbTe. *J. Jpn Inst. Met.* **66,** 1063–1065 (2002).
30. Zhu, P. W. *et al.* Enhanced thermoelectric properties of PbTe alloyed with Sb_2Te_3. *J. Phys. Condens. Matter* **17,** 7319–7326 (2005).
31. Poudeu, P. F. P. *et al.* Nanostructures versus solid solutions: Low lattice thermal conductivity and enhanced thermoelectric figure of merit in $Pb_{9.6}Sb_{0.2}Te_{10-x}Se_x$ bulk materials. *J. Am. Chem. Soc.* **128,** 14347–14355 (2006).
32. Poudeu, P. F. P. *et al.* High thermoelectric figure of merit and nanostructuring in bulk p-type $Na_{1-x}Pb_mSb_yTe_{m+2}$. *Angew. Chem. Int. Edn* **45,** 3835–3839 (2006).
33. Feldman, J. L., Singh, D. J., Mazin, II, Mandrus, D. & Sales, B. C. Lattice dynamics and reduced thermal conductivity of filled skutterudites. *Phys. Rev.B* **61,** R9209–R9212 (2000).
34. Fleurial, J.-P., Caillat, T. & Borshchevsky, A. in *Proc. ICT'97 16th Int. Conf. Thermoelectrics* 1–11 (IEEE Piscataway, New Jersey, 1997).
35. Sales, B. C., Mandrus, D. & Williams, R. K. Filled skutterudite antimonides: A new class of thermoelectric materials. *Science* **272,** 1325–1328 (1996).
36. Chung, D. Y. *et al.* A new thermoelectric material: $CsBi_4Te_6$. *J. Am. Chem. Soc.* **126,** 6414–6428 (2004).
37. Shelimova, L. E. *et al.* Thermoelectric properties of $PbBi_4Te_7$-based anion-substituted layered solid solutions. *Inorg. Mater.* **40,** 1146–1152 (2004).
38. Shelimova, L. E. *et al.* Crystal structures and thermoelectric properties of layered compounds in the ATe-Bi_2Te_3 (A = Ge, Sn, Pb) systems. *Inorg. Mater.* **40,** 451–460 (2004).
39. Kanatzidis, M. G. Structural evolution and phase homologies for "design" and prediction of solid-state compounds. *Acc. Chem. Res.* **38,** 359–368 (2005).
40. Kurosaki, K., Kosuga, A., Muta, H., Uno, M. & Yamanaka, S. Ag_9TlTe_5: A high-performance thermoelectric bulk material with extremely low thermal conductivity. *Appl. Phys. Lett.* **87,** 061919 (2005).
41. Wolfing, B., Kloc, C., Teubner, J. & Bucher, E. High performance thermoelectric Tl_9BiTe_6 with an extremely low thermal conductivity. *Phys. Rev. Lett.* **86,** 4350–4353 (2001).
42. Toberer, E. S., Sasaki, K. A., Chisholm, C. R. I., Haile, S. M. & Snyder, G. J. Local structure of interstitial Zn in β-Zn_4Sb_3. *Phys. Status Solidi* **1,** 253–255 (2007).

43. Chalfin, E., Lu, H. X. & Dieckmann, R. Cation tracer diffusion in the thermoelectric materials $Cu_3Mo_6Se_8$ and "beta-Zn_4Sb_3". *Solid State Ionics* **178,** 447–456 (2007).
44. Kim, H. J., Božin, E. S., Haile, S. M., Snyder, G. J. & Billinge, S. J. L. Nanoscale alpha-structural domains in the phonon-glass thermoelectric material beta-Zn_4Sb_3. *Phys. Rev. B* **75,** 134103 (2007).
45. Brown, S. R., Kauzlarich, S. M., Gascoin, F. & Snyder, G. J. $Yb_{14}MnSb_{11}$: New high efficiency thermoelectric material for power generation. *Chem. Mater.* **18,** 1873–1877 (2006).
46. Kauzlarich, S. M., Brown, S. R. & Snyder, G. J. Zintl phases for thermoelectric devices. *Dalton Trans.* 2099–2107 (2007).
47. Cava, R. J. Structural chemistry and the local charge picture of copper-oxide superconductors. *Science* **247,** 656–662 (1990).
48. Terasaki, I., Sasago, Y. & Uchinokura, K. Large thermoelectric power in $NaCo_2O_4$ single crystals. *Phys. Rev.B* **56,** 12685–12687 (1997).
49. Shin, W. & Murayama, N. Thermoelectric properties of (Bi,Pb)-Sr-Co-O oxide. *J. Mater. Res.* **15,** 382–386 (2000).
50. Wang, Y. Y., Rogado, N. S., Cava, R. J. & Ong, N. P. Spin entropy as the likely source of enhanced thermopower in $Na_xCo_2O_4$. *Nature* **423,** 425–428 (2003).
51. Gascoin, F., Ottensmann, S., Stark, D., Haile, S. M. & Snyder, G. J. Zintl phases as thermoelectric materials: Tuned transport properties of the compounds $Ca_xYb_{1-x}Zn_2Sb_2$. *Adv. Funct. Mater.* **15,** 1860–1864 (2005).
52. Yao, T. Thermal-Properties of AlAs/GaAs Superlattices. *Appl. Phys. Lett.* **51,** 1798–1800 (1987).
53. Touzelbaev, M. N., Zhou, P., Venkatasubramanian, R. & Goodson, K. E. Thermal characterization of Bi_2Te_3/Sb_2Te_3 superlattices. *J. Appl. Phys.* **90,** 763–767 (2001).
54. Caylor, J. C., Coonley, K., Stuart, J., Colpitts, T. & Venkatasubramanian, R. Enhanced thermoelectric performance in PbTe-based superlattice structures from reduction of lattice thermal conductivity. *Appl. Phys. Lett.* **87,** 23105 (2005).
55. Beyer, H. *et al.* High thermoelectric figure of merit *ZT* in PbTe and Bi_2Te_3-based superlattices by a reduction of the thermal conductivity. *Physica E* **13,** 965–968 (2002).
56. Hochbaum, A. I. *et al.* Enhanced thermoelectric performance of rough silicon nanowires. *Nature* **451,** 163–167 (2008).
57. Boukai, A. I. *et al.* Silicon nanowires as efficient thermoelectric materials. *Nature* **451,** 168–171 (2008).
58. Cahill, D. G., Watson, S. K. & Pohl, R. O. Lower limit to thermal conductivity of disordered crystals. *Phys. Rev. B* **46,** 6131–40 (1992).
59. Kim, W. *et al.* Cross-plane lattice and electronic thermal conductivities of ErAs: InGaAs/InGaAlAs superlattices. *Appl. Phys. Lett.* **88,** 242107 (2006).
60. Kim, W. *et al.* Thermal conductivity reduction and thermoelectric figure of merit increase by embedding nanoparticles in crystalline semiconductors. *Phys. Rev. Lett.* **96,** 045901 (2006).
61. Chiritescu, C. *et al.* Ultralow thermal conductivity in disordered, layered WSe_2 crystals. *Science* **315,** 351–353 (2007).
62. Rowe, D. M., Shukla, V. S. & Savvides, N. Phonon-scattering at grain-boundaries in heavily doped fine-grained silicon-germanium alloys. *Nature* **290,** 765–766 (1981).
63. Vining, C. B., Laskow, W., Hanson, J. O., Vanderbeck, R. R. & Gorsuch, P. D. Thermoelectric properties of pressure-sintered $Si_{0.8}Ge_{0.2}$ thermoelectric alloys. *J. Appl. Phys.* **69,** 4333–4340 (1991).
64. Jang, K.-W. & Lee, D.-H. in *Fourteenth International Conference on Thermoelectrics* 108 (IEEE, 1995).
65. Goldsmid, H. J. & Penn, A. W. Boundary scattering of phonons in solid solutions. *Phys. Lett. A* **27,** 523–524 (1968).
66. Liebmann, W. K. & Miller, E. A. Preparation phase-boundary energies, and thermoelectric properties of Insb-Sb eutectic alloys with ordered microstructures. *J. Appl. Phys.* **34,** 2653–2659 (1963).
67. Ikeda, T. *et al.* Solidification processing of alloys in the pseudo-binary PbTe–Sb_2Te_3 system. *Acta Mater.* **55,** 1227–1239 (2007).
68. Aliev, M. I., Khalilova, A. A., Arsaly, D. G., Ragimov, R. N. & Tanogly, M. Electrical and thermal properties of the GaSb-$FeGa_{1.3}$ eutectic. *Inorg. Mater.* **40,** 331–335 (2004).
69. Skrabek, E. A. & Trimmer, D. S. in *CRC Handbook of Thermoelectrics* (ed. Rowe, D. M.) 267–275 (CRC, Boca Raton, 1995).
70. Cook, B. A., Kramer, M. J., Wei, X., Harringa, J. L. & Levin, E. M. Nature of the cubic to rhombohedral structural transformation in $(AgSbTe_2)_{15}(GeTe)_{85}$ thermoelectric material. *J. Appl. Phys.* **101,** 053715 (2007).
71. Chen, N. *et al.* Macroscopic thermoelectric inhomogeneities in $(AgSbTe_2)_x(PbTe)_{1-x}$. *App. Phys. Lett.* **87,** 171903 (2005).
72. Androulakis, J. *et al.* Nanostructuring and high thermoelectric efficiency in p-type $Ag(Pb_{1-y}Sn_y)_mSbTe_{2+m}$. *Adv. Mater.* **18,** 1170–1173 (2006).
73. Hsu, K. F. *et al.* Cubic $AgPb_mSbTe_{2+m}$: Bulk thermoelectric materials with high figure of merit. *Science* **303,** 818–821 (2004).
74. Sootsman, J. R., Pcionek, R. J., Kong, H. J., Uher, C. & Kanatzidis, M. G. Strong reduction of thermal conductivity in nanostructured PbTe prepared by matrix encapsulation. *Chem. Mater.* **18,** 4993–4995 (2006).
75. Ikeda, T. *et al.* Solidification processing of alloys in the pseudo-binary PbTe-Sb_2Te_3 system. *Acta Mater.* **55,** 1227–1239 (2007).
76. Ikeda, T. *et al.* Self-assembled nanometer lamellae of thermoelectric PbTe and Sb_2Te_3 with epitaxy-like interfaces. *Chem. Mater.* **19,** 763–767 (2007).
77. Clavagueramora, M. T., Surinach, S., Baro, M. D. & Clavaguera, N. Thermally activated crystallization of $(GeSe_2)_{70}$ $(Sb_2Te_3)_{20}(GeTe)_{10}$ alloy glass - morphological and calorimetric study. *J. Mater. Sci.* **18,** 1381–1388 (1983).
78. Rowe, D. M. & Min, G. Alpha-plot in sigma-plot as a thermoelectric-material performance indicator. *J. Mater. Sci. Lett.* **14,** 617–619 (1995).
79. Toberer, E. S., Christensen, M., Iversen, B. B. & Snyder, G. J. High temperature thermoelectric efficiency in $Ba_8Ga_{16}Ge_{30}$. *Phys. Rev. B* (in the press).
80. Caillat, T., Fleurial, J. P. & Borshchevsky, A. Preparation and thermoelectric properties of semiconducting Zn_4Sb_3. *J. Phys. Chem. Solids* **58,** 1119–1125 (1997).
81. Gelbstein, Y., Dashevsky, Z. & Dariel, M. P. High performance n-type PbTe-based materials for thermoelectric applications. *Physica B* **363,** 196–205 (2005).
82. Vining, C. B., Laskow, W., Hanson, J. O., Vanderbeck, R. R. & Gorsuch, P. D. Thermoelectric properties of pressure-sintered $Si_{0.8}Ge_{0.2}$ thermoelectric alloys. *J. Appl. Phys.* **69,** 4333–4340 (1991).
83. Culp, S. R., Poon, S. J., Hickman, N., Tritt, T. M. & Blumm, J. Effect of substitutions on the thermoelectric figure of merit of half-Heusler phases at 800 °C. *Appl. Phys. Lett.* **88,** 042106 (2006).
84. Goldsmid, H. J. & Douglas, R. W. The use of semiconductors in thermoelectric refrigeration. *Brit. J. Appl. Phys.* **5,** 386–390 (1954).
85. Scherrer, H. & Scherrer, S. in *Thermoelectrics Handbook Macro to Nano* (ed. rowe, D. M.) Ch. 27 (CRC, Boca Raton, 2006).
86. Kutasov, V. A., Lukyanova, L. N. & Vedernikov, M. V. in *Thermoelectrics Handbook Macro to Nano* Ch. 37 (CRC, Boca Raton, 2006).
87. Kuznetsov, V. L., Kuznetsova, L. A., Kaliazin, A. E. & Rowe, D. M. High performance functionally graded and segmented Bi_2Te_3-based materials for thermoelectric power generation. *J. Mater. Sci.* **37,** 2893–2897 (2002).
88. Fritts, R. W. in *Thermoelectric Materials and Devices* (eds. Cadoff, I. B. & Miller, E.) 143–162 (Reinhold, New York, 1960).
89. Fleischmann, H., Luy, H. & Rupprecht, J. Neuere Untersuchungen an Halbleitenden IV VI-I V VI_2 Mischkristallen. *Zeitschrift Für Naturforschung A* **18,** 646–649 (1963).
90. Fleischmann, H. Wärmeleitfähigkeit, Thermokraft und Elektrische Leitfähigkeit von Halbleitenden Mischkristallen Der Form $(A^{I}_{x/2}\ Bi^{IV}_{1-x}C^{V}_{x/2})D^{VI}$. *Zeitschrift Für Naturforschung A* **16,** 765–780 (1961).
91. Yim, W. M. & Amith, A. Bi-Sb alloys for magneto-thermoelectric and thermomagnetic cooling. *Solid State Electron.* **15,** 1141 (1972).
92. Sidorenko, N. A. & Ivanova, L. D. Bi-Sb solid solutions: Potential materials for high-efficiency thermoelectric cooling to below 180 K. *Inorg. Mater.* **37,** 331–335 (2001).
93. Snyder, G. J. Application of the compatibility factor to the design of segmented and cascaded thermoelectric generators. *Appl. Phys. Lett.* **84,** 2436–2438 (2004).
94. Müller, E., Drasar, C., Schilz, J. & Kaysser, W. A. Functionally graded materials for sensor and energy applications. *Mater. Sci. Eng. A* **362,** 17–39 (2003).
95. Snyder, G. J. in *Thermoelectrics Handbook Macro to Nano* (ed. Rowe, D. M.) Ch. 9 (CRC, Boca Raton, 2006).
96. Snyder, G. J. & Ursell, T. Thermoelectric efficiency and compatibility. *Phys. Rev. Lett.* **91,** 148301 (2003).
97. Ursell, T. S. & Snyder, G. J. in *Twenty-first International Conference on Thermoelectrics* ICT'02 412 (IEEE, Long Beach, California, USA, 2002).

Acknowledgements

We thank Jean-Pierre Fleurial and Thierry Caillat for discussions concerning skutterudites, Marlow Industries, Cronin Vining, Yaniv Gelbstein, Ken Kurosaki for data and discussions and JPL-NASA and the Beckman Institute at Caltech for funding.